INTERNATIONAL JOURNAL FOR NUMERICAL METHODS IN FLUIDS, VOL. 8, 369–385 (1988)

TRANSIENT THREE-DIMENSIONAL FLOW IN AN ENCLOSURE WITH A HOT SPOT ON A VERTICAL WALL

D. KUHN AND P. H. OOSTHUIZEN

Department of Mechanical Engineering, Queen's University, Kingston, Ontario, Canada, K7L 3N6

KEY WORDS 3D flow Vector potential/vorticity vector Finite difference method

SUMMARY

A numerical method for the solution of the vector potential/vorticity vector formulation of the transient, fully three-dimensional Navier–Stokes energy and continuity equations has been applied to simulate the development of natural convective flow within a 'box' after a sudden temperature change on a vertical portion of the wall. Only one cavity size has been considered, this having a vertical height of three times its width and a horizontal length of six times its width. A single heated rectangular hot spot or 'element' on an otherwise adiabatic wall is centred between the vertical end walls. The opposite vertical wall is held at the intial fluid temperature, and all other walls are assumed to be adiabatic. Fluid properties have been assumed constant except for the density change with temperature that gives rise to the buoyancy force. The numerical method is an underrelaxation Gauss–Seidel method using finite differencing at each time step. Solutions have been obtained for a Prandtl number of 0·71, for Rayleigh numbers, based on the width, of between 0 and 100000 and for a number of heated element locations and sizes.

INTRODUCTION

The present work involves a numerical study of three-dimensional unsteady natural convective flow and heat transfer within a rectangular cavity or 'box' which has one vertical side partially heated and the opposite vertical side kept at a lower uniform temperature. Only one cavity size has been considered, this being shown in Figure 1. A single heated hot spot or element is symmetrically located about the vertical centreline of the partially heated wall as indicated in Figure 2. It has been assumed that the fluid in the cavity is initially at a uniform temperature and motionless. Then, at time zero, a rectangular portion of one vertical wall is heated to a uniform temperature which is higher than the initial fluid temperature, while the opposite vertical wall is kept at the initial fluid temperature, the remaining wall surfaces being assumed to be adiabatic. The effect of the heated element location and of Rayleigh number on the heat transfer rate from the elements has been considered. A comparison with corresponding two-dimensional results has also been made. A fully heated vertical wall case in a $2 \times 1 \times 1$ enclosure has briefly been considered in order to compare the results given by the present method with previous results.

Three-dimensional natural convective flow in a cavity has recently received increased attention. A number of procedures have been developed to solve three-dimensional natural convective problems, either solving the primitive or vector potential/vorticity vector formulation of the governing equations. Most available studies have been concerned with the case where the bottom

0271–2091/88/040369–17$08.50

Received 1 December 1986
Revised 14 April 1987

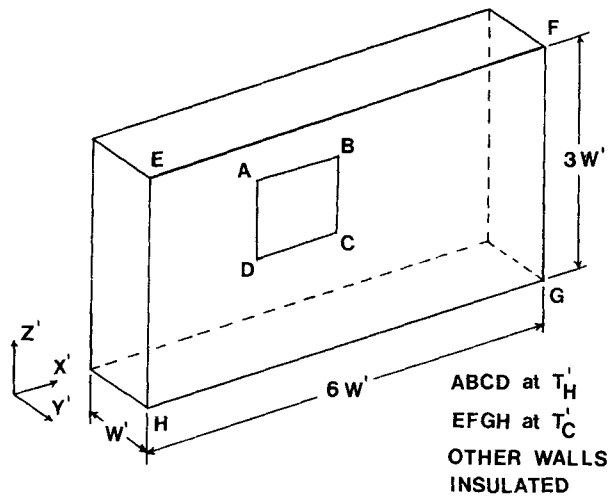

Figure 1. Three-dimensional flow situation considered

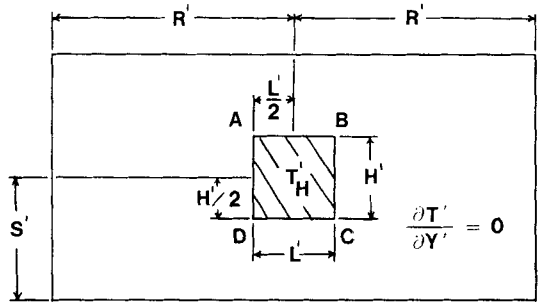

Figure 2. Heated element configuration

wall of the cavity is uniformly heated; e.g., see References 1–5. Three-dimensional natural convective flow in a cavity with the vertical walls heated to different temperatures has been investigated by Mallinson and de Vahl Davis[6] and more recently by Viskanta *et al.*[7] and Yang *et al.*,[8] a transient solution for this case being given by Chan and Banerjee.[9] No solutions for transient three-dimensional natural convective flow in a rectangular cavity with one partially heated vertical wall appear to be available. Since, as discussed below, this situation is of some practical interest, the present study was undertaken.

The motivation for the present study stems from the fact that circuit boards on which electronic components are attached are often mounted in what can be approximately modelled as a rectangular cavity. Now the performance and life of microelectronic components are strongly temperature-dependent and for proper operation they must be maintained within a specific temperature range.[10] Following start-up, the natural convective heat transfer from a heated vertical surface may be expected to pass through a number of minima and maxima before a steady state is achieved. Hence the transient development of the heat transfer rate may be of importance in the natural convective cooling of electronic equipment. It is also to be expected that the end wall effects and the effects of the finite width of the heated element may influence the heat transfer rates both during the transient state and in the steady state. A transient, fully three-dimensional solution has therefore been investigated in the present study.

GOVERNING EQUATIONS

The study is based on the use of the unsteady three-dimensional Navier–Stokes, energy and continuity equations. It has been assumed that dissipation is negligible and that the fluid properties are constant except for the density change with temperature that gives rise to the buoyancy force, this being treated by the Boussinesq approximation.

The vector potential/vorticity vector formulation of the governing equations has been considered, where, as usual, the vector potential and vorticity vector are defined as follows:

$$u' = \frac{\partial \psi'_z}{\partial y'} - \frac{\partial \psi'_y}{\partial z'}, \quad v' = \frac{\partial \psi'_x}{\partial z'} - \frac{\partial \psi'_z}{\partial x'}, \quad w' = \frac{\partial \psi'_y}{\partial x'} - \frac{\partial \psi'_x}{\partial y'}, \tag{1}$$

$$\phi'_x = \frac{\partial w'}{\partial y'} - \frac{\partial v'}{\partial z'}, \quad \phi'_y = \frac{\partial u'}{\partial z'} - \frac{\partial w'}{\partial x'}, \quad \phi'_z = \frac{\partial v'}{\partial x'} - \frac{\partial u'}{\partial y'}. \tag{2}$$

The following dimensionless variables are then introduced:

$$\begin{gathered}
\psi_x = \frac{\psi'_x}{\alpha}, \quad \psi_y = \frac{\psi'_y}{\alpha}, \quad \psi_z = \frac{\psi'_z}{\alpha}, \\
\phi_x = \frac{\phi'_x W'^2}{\alpha}, \quad \phi_y = \frac{\phi'_y W'^2}{\alpha}, \quad \phi_z = \frac{\phi'_z W'^2}{\alpha}, \\
u = \frac{u' W'}{\alpha}, \quad v = \frac{v' W'}{\alpha}, \quad w = \frac{w' W'}{\alpha}, \\
T = \frac{T' - T'_C}{T'_H - T'_C}, \quad t = \frac{vt'}{W'^2},
\end{gathered} \tag{3}$$

where ′ denotes a dimensional quantity.

In terms of these variables the governing equations are

$$\phi_x = -\left(\frac{\partial^2 \psi_x}{\partial x^2} + \frac{\partial^2 \psi_x}{\partial y^2} + \frac{\partial^2 \psi_x}{\partial z^2}\right), \tag{4}$$

$$\phi_y = -\left(\frac{\partial^2 \psi_y}{\partial x^2} + \frac{\partial^2 \psi_y}{\partial y^2} + \frac{\partial^2 \psi_y}{\partial z^2}\right), \tag{5}$$

$$\phi_z = -\left(\frac{\partial^2 \psi_z}{\partial x^2} + \frac{\partial^2 \psi_z}{\partial y^2} + \frac{\partial^2 \psi_z}{\partial z^2}\right), \tag{6}$$

$$\begin{aligned}
&Pr\frac{\partial \phi_x}{\partial t} + \frac{\partial v \phi_x}{\partial y} + \frac{\partial w \phi_x}{\partial z} - \frac{\partial u \phi_y}{\partial y} - \frac{\partial u \phi_z}{\partial z} \\
&= Pr\left(\frac{\partial^2 \phi_x}{\partial x^2} + \frac{\partial^2 \phi_x}{\partial y^2} + \frac{\partial^2 \phi_x}{\partial z^2}\right) + Ra\,Pr\frac{\partial T}{\partial y},
\end{aligned} \tag{7}$$

$$\begin{aligned}
&Pr\frac{\partial \phi_y}{\partial t} + \frac{\partial u \phi_y}{\partial x} + \frac{\partial w \phi_y}{\partial z} - \frac{\partial v \phi_x}{\partial x} - \frac{\partial v \phi_z}{\partial z} \\
&= Pr\left(\frac{\partial^2 \phi_y}{\partial x^2} + \frac{\partial^2 \phi_y}{\partial y^2} + \frac{\partial^2 \phi_y}{\partial z^2}\right) - Ra\,Pr\frac{\partial T}{\partial x},
\end{aligned} \tag{8}$$

$$Pr\frac{\partial \phi_z}{\partial t} + \frac{\partial u \phi_z}{\partial x} + \frac{\partial v \phi_z}{\partial y} - \frac{\partial w \phi_x}{\partial x} - \frac{\partial w \phi_y}{\partial y}$$

$$= Pr\left(\frac{\partial^2 \phi_z}{\partial x^2} + \frac{\partial^2 \phi_z}{\partial y^2} + \frac{\partial^2 \phi_z}{\partial z^2}\right), \tag{9}$$

$$Pr\frac{\partial T}{\partial t} + \frac{\partial uT}{\partial x} + \frac{\partial vT}{\partial y} + \frac{\partial wT}{\partial z}$$

$$= \left(\frac{\partial^2 T}{\partial x^2} + \frac{\partial^2 T}{\partial y^2} + \frac{\partial^2 T}{\partial z^2}\right), \tag{10}$$

$$u = \frac{\partial \psi_z}{\partial y} - \frac{\partial \psi_y}{\partial z}, \quad v = \frac{\partial \psi_x}{\partial z} - \frac{\partial \psi_z}{\partial x}, \quad w = \frac{\partial \psi_y}{\partial x} - \frac{\partial \psi_x}{\partial y}. \tag{11}$$

The boundary conditions on velocity and temperature follow directly from the problem description. On all walls

$$u = v = w = 0, \tag{12}$$

while for the heated wall section, the cooled wall and all the adiabatic wall sections respectively

$$T = 1, \quad T = 0, \quad \frac{\partial T}{\partial n} = 0. \tag{13}$$

As shown by Hirasaki and Hellums,[11] the vector potential boundary conditions on the end walls, i.e., at $x = 0$ and 6, are

$$\frac{\partial \psi_x}{\partial x} = \psi_y = \psi_z = 0. \tag{14}$$

Similar conditions apply on the other wall pairs, i.e., at $y = 0$ and 1 and $z = 0$ and 3. The conditions given in equation (14) will also apply on the plane of symmetry, i.e., on the yz plane at $x = 3$.

The vorticity at the wall can be determined from the vector potential; e.g., at $x = 0$

$$\phi_x = 0, \quad \phi_y = -\frac{\partial^2 \psi_y}{\partial x^2}, \quad \phi_z = -\frac{\partial^2 \psi_z}{\partial x^2}. \tag{15}$$

On the yz plane at $x = 3$ the following boundary conditions also apply:

$$u = \frac{\partial v}{\partial x} = \frac{\partial w}{\partial x} = 0, \quad \frac{\partial T}{\partial x} = 0, \tag{16}$$

$$\frac{\partial \psi_x}{\partial x} = \psi_y = \psi_z = 0, \quad \frac{\partial \phi_x}{\partial x} = \phi_y = \phi_z = 0. \tag{17}$$

The initial conditions are

$$t = 0, \quad T = 0, \quad \psi_x = \psi_y = \psi_z = 0, \quad \phi_x = \phi_y = \phi_z = 0. \tag{18}$$

SOLUTION PROCEDURE

In the above equations the spatial derivatives have been approximated by second-order central differencing at all internal points and by second-order forward or backward differencing at points on the solid boundaries and on the plane of symmetry. All time derivatives have been approximated by first-order backward differencing. The resulting equations were then solved using an underrelaxation Gauss–Seidel technique with iteration at each time step. The solution

procedure adopted here for the three-dimensional flow is basically an extension of the procedure developed in Reference 12 for two-dimensional problems and broadly similiar to that used in Reference 13.

Hence equations (4)–(17) can be written in the following form:

$$G_{i,j,k} = a_1 G_{i+1,j,k} + a_2 G_{i-1,j,k} + a_3 G_{i,j+1,k} + a_4 G_{i,j-1,k} + a_5 G_{i,j,k+1} + a_6 G_{i,j,k-1} + a_7 = F_n, \quad (19)$$

where G represents any of u, v, w, T, ψ_i or ϕ_i and some of the coefficients are zero for points on the boundary. Equation (15) is simplified using the zero-velocity condition at the wall and the definition of ψ_i before being written in the form of equation (19). Since a transient problem is being considered, the coefficient a_7, for cases where G represents T or ϕ_i, includes the contribution of the $G_{i,j,k}$ at the beginning of the time step. Equation (19) written in the form

$$G^1_{i,j,k} = G^0_{i+1,j,k} + w_n(F^0_n) \quad (20)$$

in applied to all points, where w_n is a relaxation factor, F_n represents the right-hand side of equation (19) and superscripts 0 and 1 indicate conditions at the beginning and the end of the iteration step respectively. The fluid variables are determined by systematically applying equation (20), using the latest calculated values, along points in a row, then along successive rows in a plane and finally along successive planes within the volume.

Equation (20) forms the basis of the solution procedure. At time zero, the conditions at all internal points are given by the initial conditions given in equation (18). In advancing to time Δt, these conditions are taken as the 'first guess' at conditions at this time at all internal points. The boundary conditions known at time Δt are also set. The solution procedure then advances essentially as follows:

(i) The internal temperature values are determined.
(ii) Unknown temperature values on the boundaries are determined.
(iii) The above steps are repeated a second and third time. (The repetition of the above steps is discussed more fully below.)
(iv) Internal vorticity vector values are determined.
(v) Unknown vorticity vector values on the boundaries are determined.
(vi) Steps (iv) and (v) are repeated a second and third time.
(vii) Internal vector potential values are determined.
(viii) Unknown vector potential values on the boundaries are determined.
(ix) Velocity values are determined.
(x) Steps (vii)–(ix) are repeated a second and third time.
(xi) Convergence of the value of the temperature is checked.
(xii) If convergence is not achieved, step (i)–(xi) are repeated until convergence.
(xiii) This gives the solution at the end of the time step.

This solution was advanced through the next time step using the same procedure and so on.

At the end of each time step the local transfer rates over the heated element are derived from the temperature distribution using second-order differencing. The average heat transfer rate from the heated element was then determined by numerically integrating the local heat transfer rates over the heated element using Simpson's rule. The boundary of the heated element was taken as halfway between the grid points with boundary conditions $T = 1$ and $\partial T/\partial y = 0$.

The repeated calculation of the cycle of each fluid variable field before beginning the solution of the next field has been implemented within the procedure to aid convergence while using a relatively large time step, i.e., $\Delta t = 0{\cdot}0005$. Test runs of the procedure using a different number of cycles per solution indicate that three cycles per solution of each field optimally aids convergence at

each time step. The results from test runs using more than three cycles closely agree with the three cycle results, but these solutions require more time to converge. At least three cycles per solution were needed while using a dimensionless time step of 0·0005, it being found that results using fewer cycles disagree sharply with the three-cycle results.

The above procedure was solved using an IBM3081. Typically the transient solution of the governing equations from the initial conditions to the assumed steady state, $t = 0{\cdot}4$, required 5000 iterations for a Rayleigh number range of between 0 and 100000. Between 3 and 18 iterations were required for convergence at each time step, with each iteration requiring approximately 3·8 CPU seconds.

RESULTS

The solution has as parameters:

(i) the Rayleigh number Ra which is based on the width W' of the cavity;
(ii) the dimensionless position of the heated element as defined by (R, S) (see Figure 2);
(iii) the dimensionless size of the heated elements as defined by (L, H) (see Figure 2);
(iv) the Prandtl number Pr of the fluid in the cavity;
(v) the relative dimensions of the cavity.

As already mentioned, results have only been obtained for a cavity of size $6 \times 1 \times 3$ as defined in Figure 1. A single dimensionless element size of $(L, H) = (0{\cdot}716, 0{\cdot}333)$ has been considered, elements being centred between the adiabatic end walls at $x = 3$. These results have only been obtained for $Pr = 0{\cdot}71$. The convergence criterion at each time step was

$$\left| \frac{T^n - T^{n-1}}{T^n} \right| < 0{\cdot}005,$$

where n denotes the iteration number. $22 \times 15 \times 37$ uniformly spaced grid points were used.

In studying the dependence of the results on grid size, attention was directed to the mean temporal Nusselt number extrema values (see later) for a centrally located element. The results were found to be most sensitive to the grid size in the x direction. Hence three grids differing in size in the x direction were considered, and from these results extrapolated extrema results for a zero grid size were determined and compared with the results determined using the $22 \times 15 \times 37$ grid. The extrema results were found to occur at dimensionless times that agreed to within 3% of each other, and the Nusselt numbers at these extrema values agreed to within 3% of each other.

A comparison of the present results with the corresponding two-dimensional results and with the steady state results of Mallinson and de Vahl Davis[6] is of interest. In this problem a cavity of size $2 \times 1 \times 1$ has been considered. The variation of the dimensionless heat transfer rate Nu and the absolute maximum values $|\psi_i|_{\max}$ of the components of the vector potential with dimensionless time are given in Figures 3 and 4 respectively. If the variations of the flow quantities in the x direction are negligible, a two-dimensional flow will of course exist in the cavity. It may be shown that under the two-dimensional assumption the y and z components of the vector potential become zero and the x component becomes identically the stream function used in the two-dimensional analysis. Hence the difference between the variation of $|\psi_x|_{\max}$ and $|\psi_{2D}|_{\max}$ shown in Figure 4 illustrates the influence of the end walls on the fluid flow. Figure 3 shows that two- and three-dimensional results for the variation of Nu with time agree closely. The largest differences in Nu values occur at early times. During this period the fluid motion is largely parallel to the unheated end walls, i.e., there is little fluid motion in the x direction. However, the fluid is slowed by the end walls, which accounts for the lower Nu values predicted for the three-dimensional case as

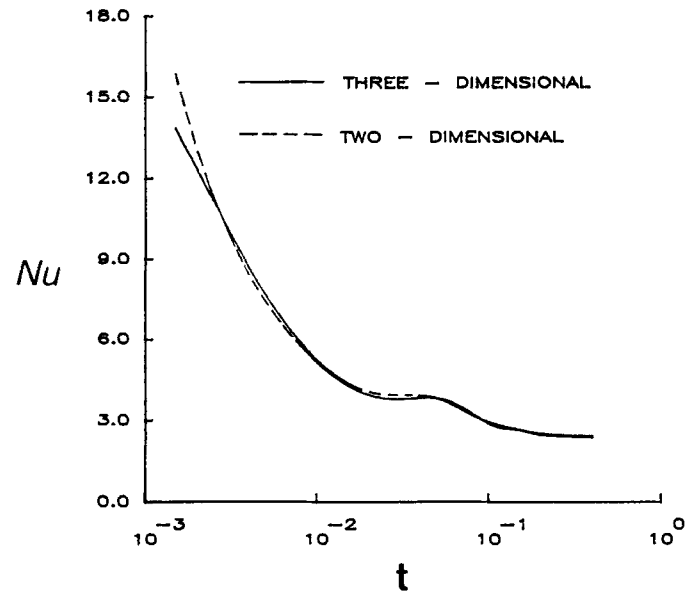

Figure 3. Nusselt number variation with dimensionless time for the two- and three-dimensional case of a fully heated vertical wall within a cavity of size 2 × 1 × 1

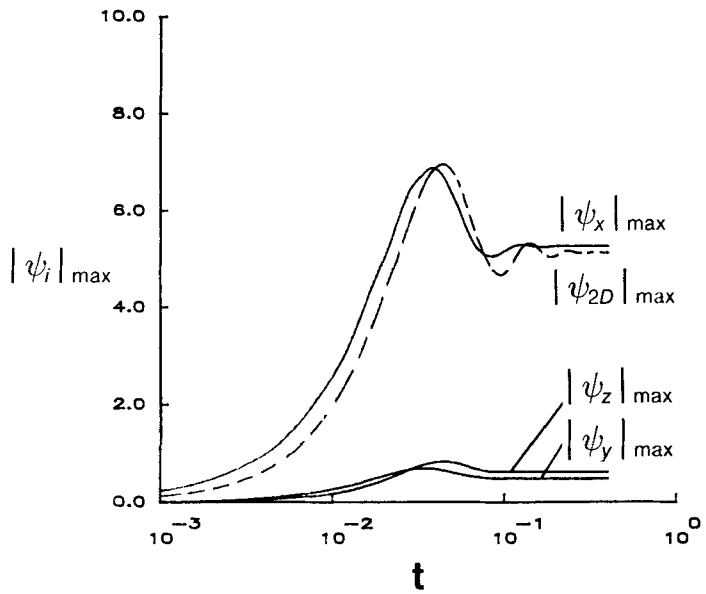

Figure 4. Variation of the absolute maximum value of the components of the vector potential with dimensionless time for the two- and three-dimensional case of a fully heated vertical wall within a cavity of size 2 × 1 × 1

compared with the two-dimensional results. As time progresses, fluid motion in the x direction becomes more intense, as may be seen by the strengthening of the absolute maximum values of the y and z components of the vector potential, and as a consequence the two- and three-dimensional variations of Nu with time become essentially the same. From Figures 4 and 5 it may be seen that at

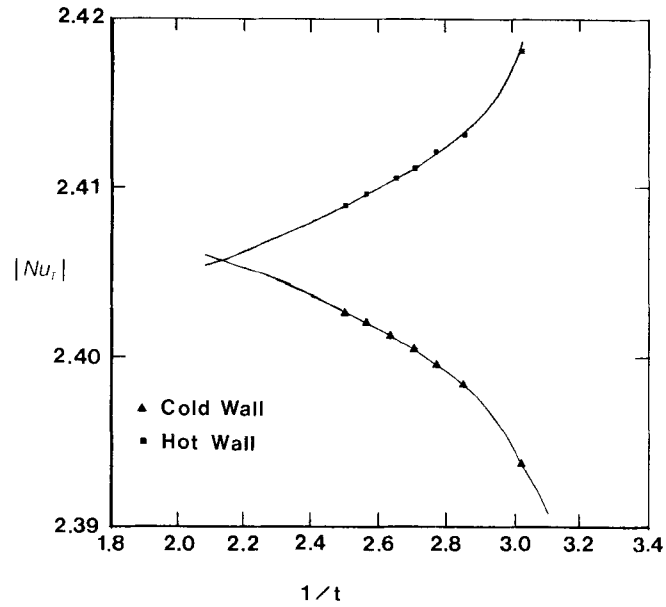

Figure 5. Variation of the absolute value of the Nusselt number with the inverse of the dimensionless time for the three-dimensional case of a fully heated vertical wall within a cavity of size 2 × 1 × 1

a dimensionless time of $t = 0{\cdot}4$ the steady state has not quite yet been reached; however, it may be expected that at this time the $|Nu_T|$ is close to the steady state value. $|Nu_T|$ is defined as the absolute value of the average heat transfer rate from an entirely heated hot or cold wall. The variation of $|Nu_T|$ with $1/t$ shown in Figure 5 predicts that the average heat transfer rate at the cold wall will become greater than at the hot wall for a period of time. The heat transfer rates from the hot and cold walls are expected to converge; however, a decaying oscillation about the final steady state value is not unexpected. Mallinson and de Vahl Davis[6] predicted an average heat transfer rate over the entire wall of 2·20 i.e., $|Nu_T| = 2{\cdot}20$, and an average heat transfer rate along the heated wall's vertical centreline of 2·32. These results compare with values predicted at $t = 0{\cdot}4$ of 2·41 and 2·51, it being noted that the differences between the two heat transfer rates are approximately the same.

The case where only a portion of the vertical wall is heated will be considered next. The heated element lies symmetrically on the centreline of the vertical wall, i.e., is centred between the end walls. The flow, as mentioned before, is therefore symmetrical about the vertical centre plane. The effect of the heated element location and Rayleigh number on the variation of Nu with dimensionless time is shown in Figures 6–9. From these figures it is clear that the three-dimensional transition to steady state, for heated elements not located near horizontal walls, consists of five distinct phases, namely:

(i) a conduction phase where Nu decreases quickly from an initial infinite value to a temporal minimum;
(ii) a short phase where Nu increases to a temporal maximum as fluid motion in the yz plane intensifies;
(iii) another short phase where Nu decreases to a less distinct temporal minimum as fluid motion in the yz plane weakens and the fluid becomes warmer;
(iv) a longer phase where Nu increases to a local temporal maximum lower than the initial maximum as three-dimensional flow becomes important;
(v) a phase where Nu slowly decreases, approaching the final steady state value.

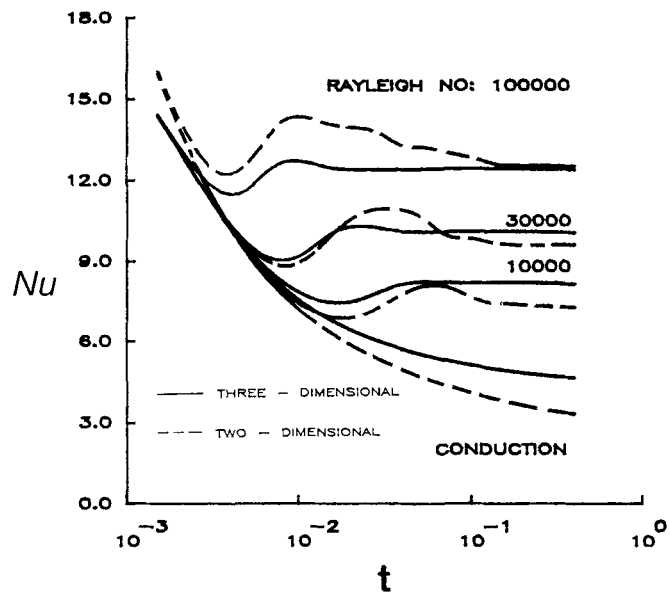

Figure 6. Comparison of the effect of Rayleigh number on the Nusselt number variation with dimensionless time for two- and three-dimensional cases, element size $L \times H = 0{\cdot}716 \times 0{\cdot}333$ and element position $(R, S) = (3, 1)$

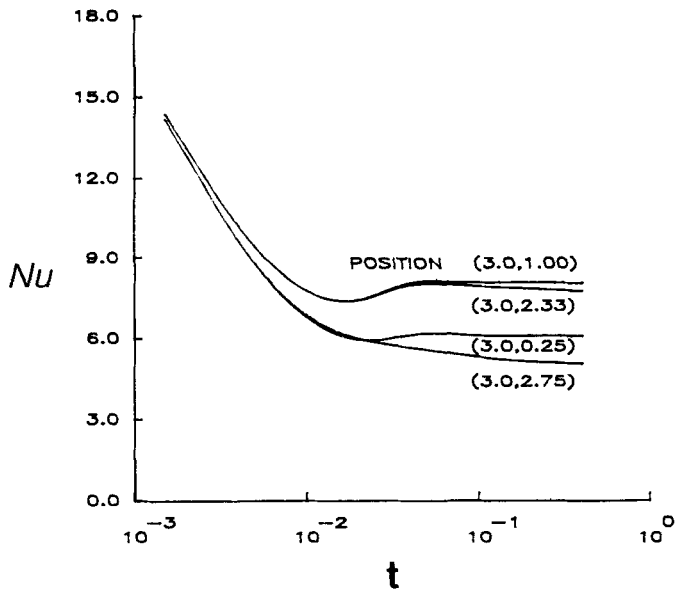

Figure 7. Comparison of the effect of position, as defined in Figure 2, on the Nusselt number variation with dimensionless time for $Ra = 10^4$ and element size $L \times H = 0{\cdot}716 \times 0{\cdot}333$

In Figures 6–9 the broken lines show the two-dimensional results, obtained from Reference 14, which correspond to the three-dimensional cases that have been considered. In these figures it may be seen that in most cases considered the steady value of Nu is higher in the three-dimensional case than in the two-dimensional case.

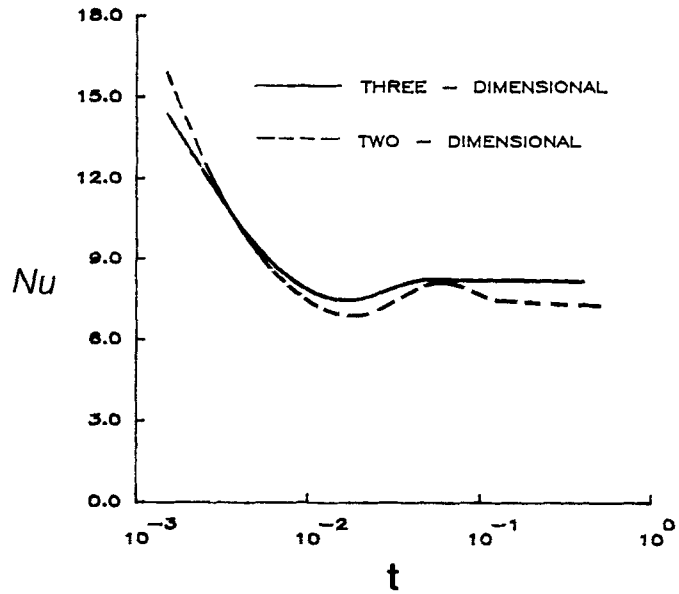

Figure 8. Comparison of two- and three-dimensional Nusselt number variations with dimensionless time for $Ra = 10^4$, element size $L \times H = 0{\cdot}716 \times 0{\cdot}333$ and element position $(R, S) = (3, 1)$

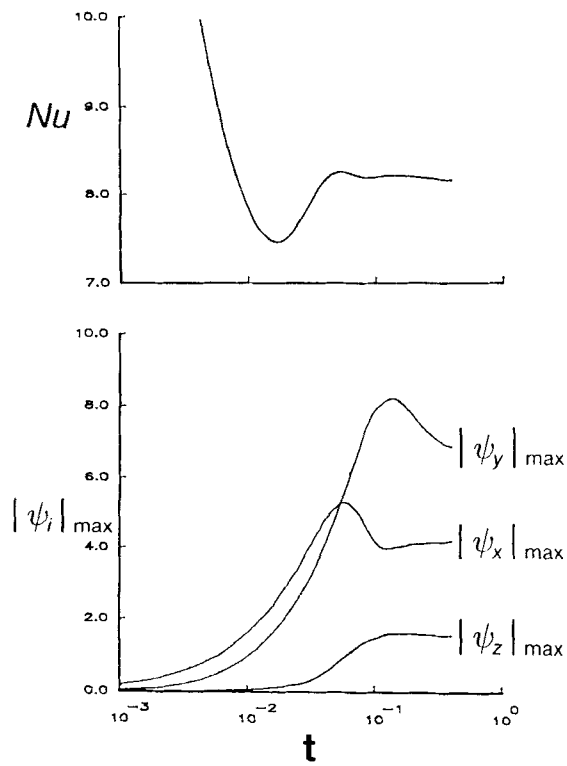

Figure 9. Transient development of the Nusselt number and the absolute maximum value of the components of the vector potential for $Ra = 10^4$, element size $L \times H = 0{\cdot}716 \times 0{\cdot}333$ and element position $(R, S) = (3, 1)$

As mentioned above, these five phases describe the transition to steady state for the three-dimensional cases where the heated element is not located near the horizontal walls. The variation of Nu with dimensionless time is more complex in the three-dimensional case than in the two-dimensional case, because in the former case the development of the motion in the x direction of course influences the variation. Figure 9 illustrates the influence of the fluid motion in the x direction on Nu for the three-dimensional case considered in Figure 8. Here the transient behaviour of Nu and the absolute maximum values of the three components of the vector potential are shown. The values of $|\psi_y|_{max}$ and $|\psi_z|_{max}$ are not negligible with respect to $|\psi_x|_{max}$, indicating strong fluid motion in the x direction. $|\psi_y|_{max}$ and $|\psi_z|_{max}$ reach maximum values as Nu reaches its second temporal maximum, implying that fluid motion in the x direction accounts for the second maximum Nu value and, as would be expected, enhances heat transfer.

The effect of the heated element location, i.e., the influence of the horizontal walls, on the variation of Nu with time is illustrated by Figure 7. It will be recalled that the dimensionless position of the heated element is defined by (R, S) (see Figure 2), where R is the horizontal distance from the end wall at $x = 0$ and S is the vertical distance from the bottom. All results for heated elements located at least two element heights away from the horizontal walls closely coincide with each other and are essentially the same as those given by the curve for position (3, 1) shown in this figure. The variation of the heat transfer rate with the element located outside of this range, however, is strongly influenced by the heated element location. Heated elements located near the top, e.g., position (3·00, 2·75), experience no temporal maximum Nu. Here there is little fluid motion, since the fluid heated by the elements is unable to rise and hence heat transfer progresses mainly by conduction. The transient heat transfer development is not as strongly effected when the element is located near the bottom wall. However, as can be noted from the curve for position (3·00, 0·25), the heat transfer is somewhat lower than for an element located far from any wall, this being due to the restriction of fluid entrainment resulting from the presence of the bottom wall. The curve for position (3·00, 2.33) further emphasizes that the variation of Nu with time is largely unaffected by the location of the heated element except when the element is located close to a horizontal wall, in particular located close to the top wall.

Attention is next turned to the distribution of the local heat transfer rate over the surface of the heated element, this local heat transfer rate being expressed as a local Nusselt number Nu_L also based on the cavity width W'. The variation of Nu_L over the surface of an element that is located relatively far from any of the cavity walls is shown in Figure 10 for times that correspond to the extrema in the average Nusselt number variations with time. At all times Nu_L is a maximum at the bottom of the heated element and a minimum at the top of the element. In all cases there is also an increase in the local heat transfer at the edges of the heated element, the distribution of Nu_L at the initial temporal minimum Nu indicating that side effects are already important at this time. Hence three-dimensional effects enhance the heat transfer rate at the sides of the element. These three-dimensional effects become more important after the initial minimum Nu indicated by the steeper constant heat flux lines in Figures 10(b)–(e). The local heat transfer rate results confirm an earlier observation that there is little change in Nu with time following the initial temporal maximum, the changes after this time being restricted to the bottom corners of the heated elements.

The effect of Rayleigh number on the effectively steady state Nu_L distribution for a heated element not located near a horizontal or side wall is given in Figure 11. In all cases, except of course for pure conduction, Nu_L is again a maximum at the bottom and a minimum at the top and increases near the edges of the elements due to three-dimensional effects. As would be expected, as Ra increases, the portion of the element over which these three-dimensional effects are important decreases; i.e., three-dimensional effects become less important and Nu_L becomes increasingly uniform over the element at the larger Ra values.

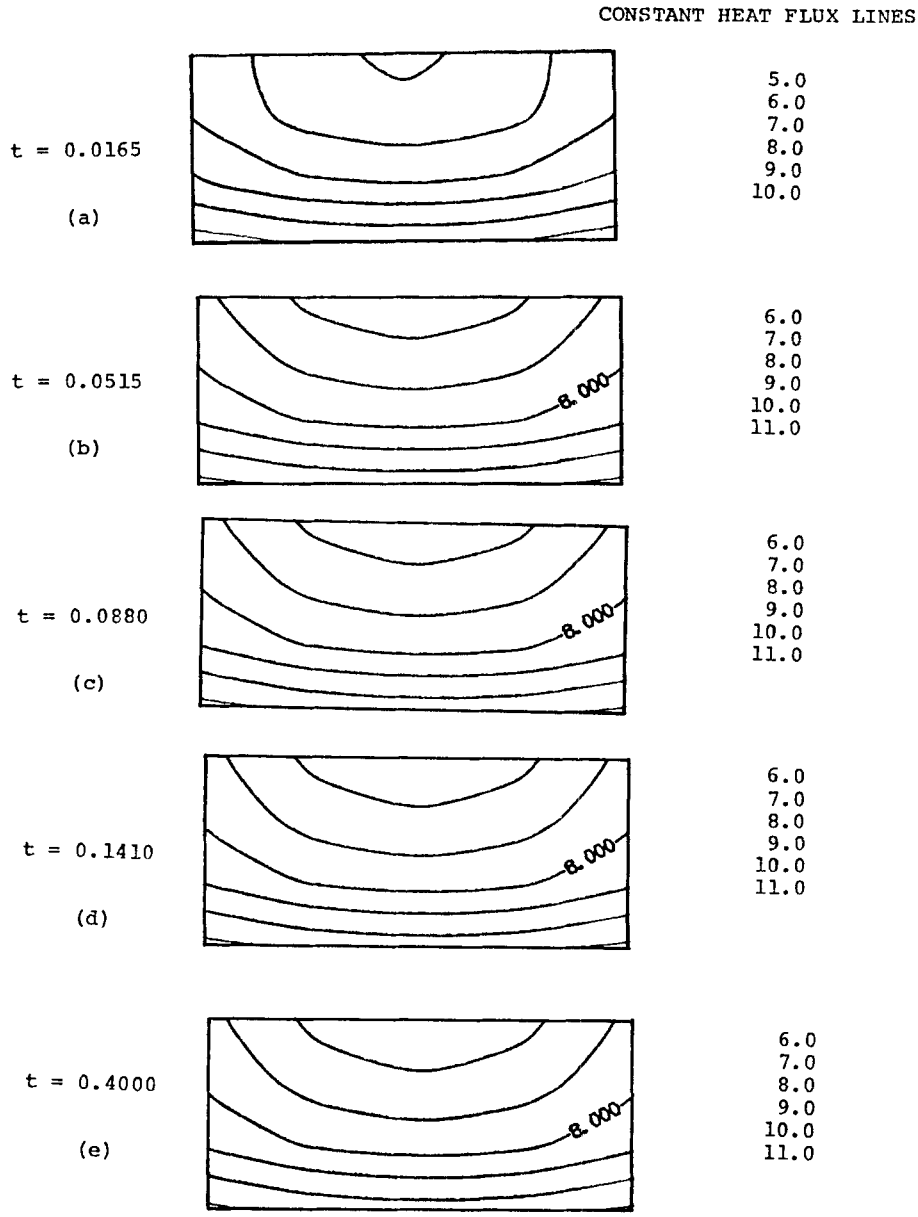

Figure 10. Transient development of the distribution of local heat transfer rate over the element for $Ra = 10^4$, element size $L \times H = 0{\cdot}716 \times 0{\cdot}333$ and element position $(R, S) = (3, 1)$

The distribution of Nu_L, is more strongly influenced by the position of the heated element than is the Nu distribution, typical distributions being given in Figure 12. A typical Nu_L distribution for elements located away from the horizontal walls is given Figure 12(b). The influence of the top wall is shown in Figure 12(a). As discussed earlier, when the element is near the top wall the heat transfer is mainly by conduction. As will be seen from Figure 12(a), the effect of the top wall is to reduce the local heat transfer rate and to reduce the three-dimensional effects. The local heat transfer distribution for an element located near the bottom wall is considered finally and is of most interest.

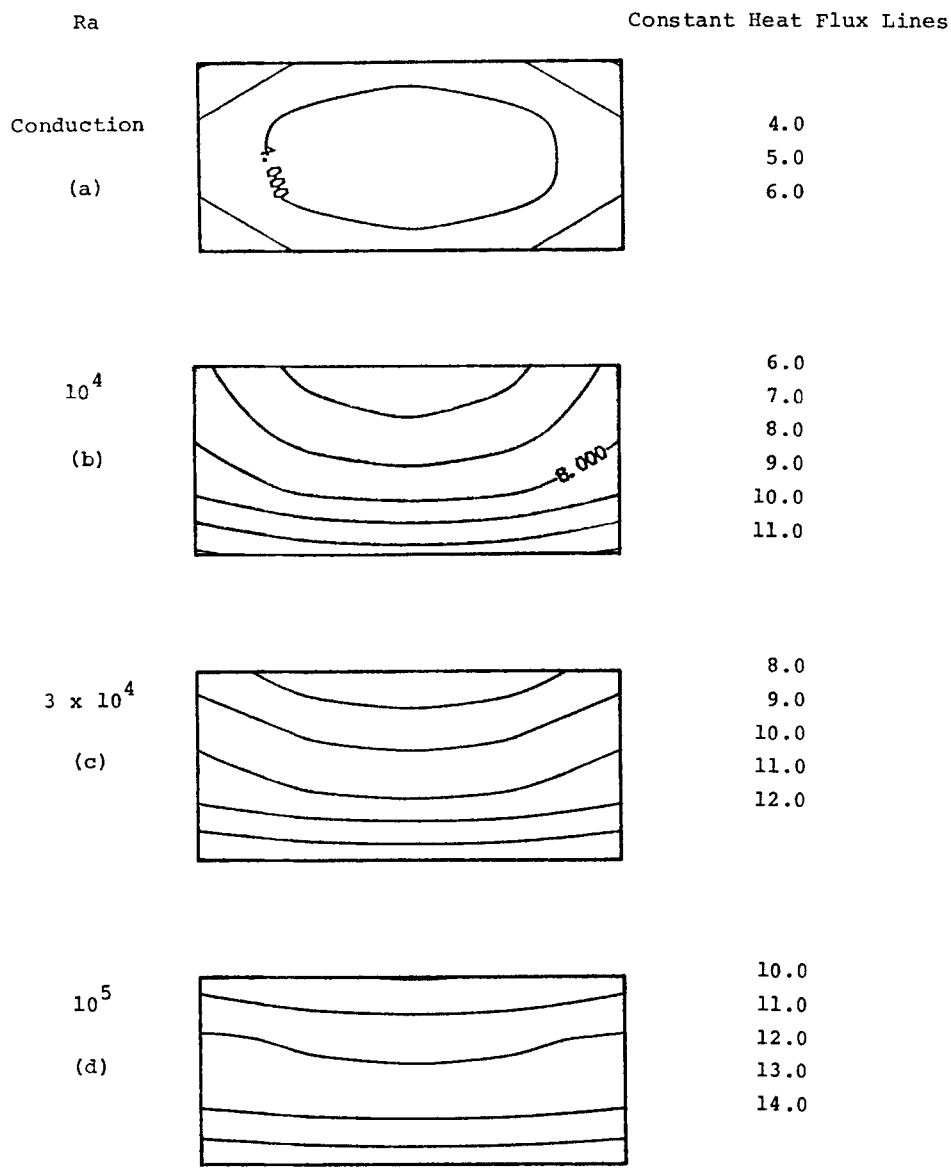

Figure 11. Effect of Rayleigh number on the distribution of local heat transfer rate over the element for dimensionless time at $t = 0{\cdot}4000$, element size $L \times H = 0{\cdot}716 \times 0{\cdot}333$ and element position $(R, S) = (3, 1)$

In this case Nu_L is almost uniform across the element, and the constant heat flux lines are vertical. The distinctive Nu_L distribution is due to the orientation of the fluid motion. Fluid entrained to cool the heated element must come forward and up and move strongly towards the vertical centre of the element. Results from a two-dimensional analysis differ most strongly from this three-dimensional case, since a two-dimensional analysis can only predict a Nu_L distribution with horizontal constant heat flux lines.

The influence of element position on fluid motion within the enclosure is further illustrated in Figure 13 by considering the variation of the maximum absolute value of the components of the

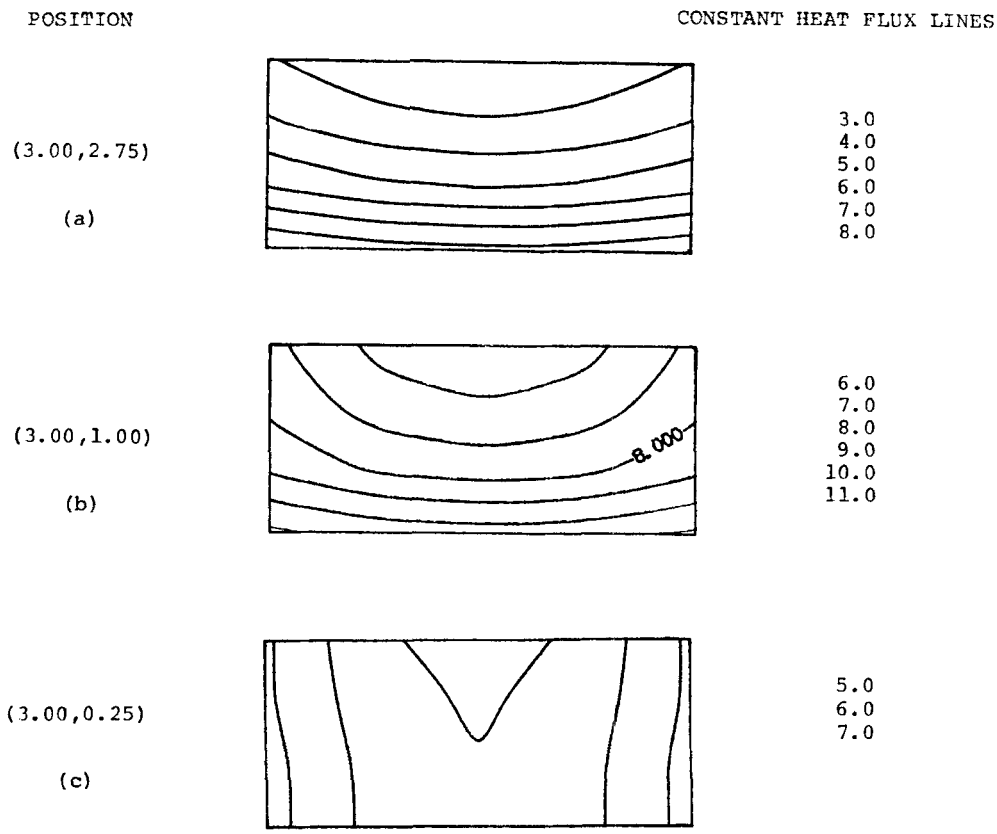

Figure 12. Effect of element position on the distribution of local heat transfer rate over the element for dimensionless time at $t = 0{\cdot}4000$, $Ra = 10^4$ and element size $L \times H = 0{\cdot}716 \times 0{\cdot}333$

vector potential with time. Figure 13(a) compares the variation of $|\psi_x|_{\max}$ with time at different element locations. Here it is seen that $|\psi_x|_{\max}$ is retarded by the presence of the horizontal walls. In Figure 13(b) it is shown that the values of $|\psi_y|_{\max}$ become larger for the element located at the bottom than for the centrally located element. This supports the earlier observation that fluid motion in the x direction plays a more important role in the heat transfer from an element located near the bottom. A comparison of the variation of $|\psi_z|_{\max}$ with time given in Figure 13(c) with that of $|\psi_x|_{\max}$ and $|\psi_y|_{\max}$ indicates $|\psi_z|_{\max}$ is essentially negligible with respect to $|\psi_x|_{\max}$ and $|\psi_y|_{\max}$ for elements not located near the top wall. The relative weakness of the vector components for the element located near the top wall in comparison with the results for elements located away from the top wall indicates, as was noted earlier, that the heat transfer from elements located near the top progresses mainly by conduction.

CONCLUSIONS

A two-dimensional solution procedure has been extended to solve the fully three-dimensional Navier–Stokes, energy and continuity equations. The solution procedure has been successfully applied to simulate the development of natural convective flow within a 'box' after a sudden temperature change on a vertical wall portion.

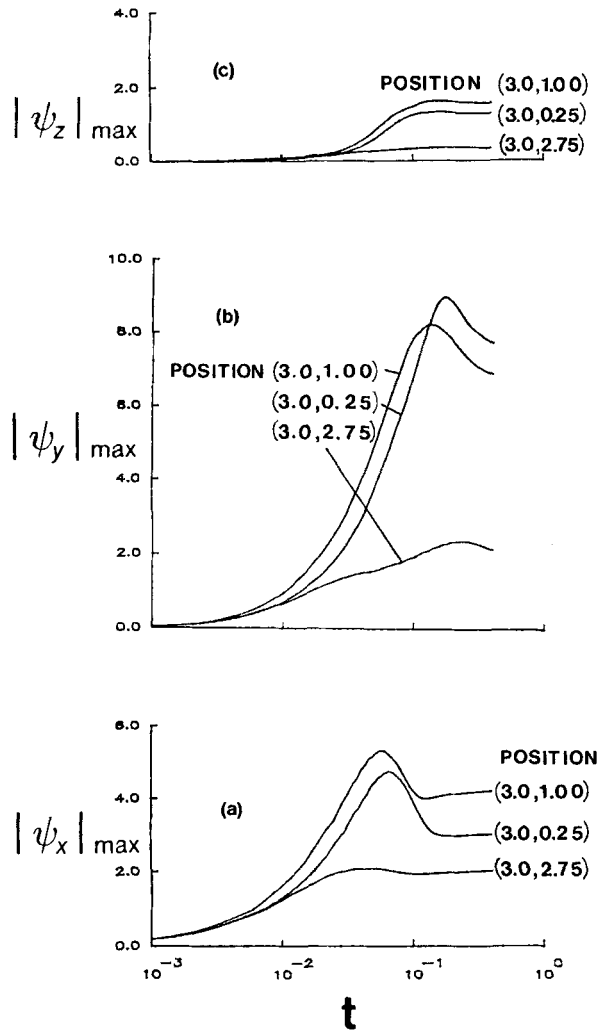

Figure 13. Effect of element position, as defined in Figure 2, on the transient development of the maximum absolute value of the components of the vector potential for $Ra = 10^4$ and element size $L \times H = 0{\cdot}716 \times 0{\cdot}333$

The results indicate that:

(i) For elements located away from the horizontal walls, the initial temporal minimum average heat transfer rate is less than the steady state value for all Rayleigh numbers considered here.

(ii) The variation of the average heat transfer rate with time is little affected by element position unless the element is located close to a horizontal wall.

(iii) The three-dimensional flow tends to increase the local heat transfer rate near the edges of the element, causing the mean heat transfer rate to be higher than that in the corresponding two-dimensional flow.

(iv) The three-dimensional analysis predicts a significantly different local Nusselt number distribution for an element located near the bottom wall than that predicted by a two-dimensional analysis.

ACKNOWLEDGEMENTS

This work was supported by the Natural Sciences and Engineering Research Council of Canada.

NOMENCLATURE

D	Domain of heated element
F_n	Right-hand side of Equation (19)
H'	Height of heated element
H	Dimensionless height of heated element ($= H'/W'$)
k	Thermal conductivity
L'	Width of heated element
L	Dimensionless width of heated element ($= L'/W'$)
Nu_L	Local Nusselt number ($q_w W'/k(T'_H - T'_C)$)
Nu	Average Nusselt number from the heated element based on $W((1/LH)\int_D Nu_L \, dx \, dz)$
$\lvert Nu_T \rvert$	Absolute value of the average Nusselt number from the entirely heated hot or cold wall based on $W'((1/2W^2)\int_0^2\int_0^1 Nu_L \, dx \, dz)$
p	Pressure
Pr	Prandtl number
q_w	Local heat transfer rate at the wall ($-k\,\partial T'/\partial y'$)
R'	Distance of heated element from end wall in x direction (see Figure 2)
R	Dimensionless distance of heated element from end wall in x direction ($= R'/W'$)
Ra	Rayleigh number
S'	Distance of heated element from bottom (see Figure 2)
S	Dimensionless distance of heated element from bottom ($= S'/W'$)
T'	Temperature
T	Dimensionless temperature (see equation (3))
t'	Time
t	Dimensionless time ($= t'v/W'^2$)
u', v', w'	Velocity components in x', y', z' directions
u, v, w	Dimensionless velocity components in x, y, z directions ($= u'W'/\alpha, v'W'/\alpha, w'W'/\alpha$)
W'	Distance between heated walls
x', y', z'	Cartesian co-ordinates as defined in Figure 1
x, y, z	Dimensionless Cartesian co-ordinates ($= x'/W', \; y'/W', \; z'/W'$)
α	Thermal diffusivity
v	Kinematic viscosity
$\phi'_x, \phi'_y, \phi'_z$	Vorticity vector components (see equation (2))
ϕ_x, ϕ_y, ϕ_z	Dimensionless vorticity vector components (see equations (4)–(6))
$\psi'_x, \psi'_y, \psi'_z$	Vector potential components (see equation (1))
ψ_x, ψ_y, ψ_z	Dimensionless vector potential components (see equation (11))
$\lvert\psi_x\rvert_{max}$	Maximum absolute value of x component of the vector potential
$\lvert\psi_y\rvert_{max}$	Maximum absolute value of y component of the vector potential
$\lvert\psi_z\rvert_{max}$	Maximum absolute value of z component of the vector potential
$\lvert\psi_{2D}\rvert_{max}$	Maximum absolute value of the stream function

Subscripts

H	Condition at the hot wall
C	Condition at the cold wall
L	Local condition

REFERENCES

1. K. Aziz and J. D. Hellums, 'Numerical solution of the three-dimensional equations of motion for laminar natural convection', *Phys. Fluids*, **10,** 314–324 (1967).
2. I. Catton, 'The effect of insulated vertical walls on the onset of motion in a fluid heated from below', *Int. J. Heat Mass Transfer*, **15,** 665–672 (1972).
3. H. Ozoe, K. Yamamato, H. Sayama and S. W. Churchill, 'Natural convection patterns in a long inclined rectangular box heated from below', *Int. J. Heat Mass Transfer*, **20,** 131–139 (1977).
4. C. D. Upson, P. M. Gresho, R. L. Sani, S. T. Chan and R. L. Lee, in T. M. Shih (ed.), 'A thermal convection simulation in three dimensions by a modified finite element method', *Numerical Properties and Methodologies in Heat Transfer*, pp. 295–259 (1983).
5. H. Ozoe, M. Hiramitsu and T. Matsui, 'Numerical calculation of three-dimensional turbulent natural convection in a cubical enclosure heated from the bottom and cooled from a portion of two adjacent vertical walls', *Int. Symp. on Heat Transfer*, Beijing, October, 1985, Paper 85-ISHI-I-3.
6. G. D. Mallinson and G. de Vahl Davis, 'Three-dimensional natural convection in a box: a numerical study', *J. Fluid Mech.*, **83** (part 1), 1–31 (1977).
7. R. Viskanta, D. M. Kim and C. Gau, 'Three-dimensional numerical natural convection heat transfer of a liquid metal in a cavity', *Int. J. Heat Mass Transfer*, **29,** 474–485 (1986).
8. H. Q. Yang, K. T. Yang and J. R. Lloyd, 'Flow transition in a laminar buoyant flow in a three-dimensional tilted rectangular enclosure', *Int. Heat Transfer Conf.*, San Francisco, August 1986.
9. A. M. C. Chan and S. Banerjee, 'Three-dimensional numerical analysis of transient natural convection in rectangular enclosures', *J. Heat Transfer*, **101,** 114–119 (1979).
10. A. H. Mayer, in S. Oktay and A. Bar-Cohen (eds), 'Heat transfer technology in the service of the integrated microelectronic revolution', *Heat Transfer in Electronic Equipment, ASMEHTD*, **28,** 1983, pp. 1–3.
11. G. J. Hirasaki and J. D. Hellums, 'A general formulation of the boundary conditions on the vector potential in three-dimensional hydrodynamics', *Q. J. Appl. Math.*, **26,** 331–342 (1968).
12. P. H. Oosthuizen and D. Kuhn, 'Unsteady free convective heat transfer through a closed square container filled with a liquid and a gas', *ASME Summer Annual Meeting*, 1984, ASME-Paper 84-HT-66.
13. J. Han, 'A computational method to solve nonlinear elliptic equations for natural convection in enclosures', *Numer. Heat Transfer*, **2,** 165–176 (1979).
14. D. Kuhn and P. H. Oosthuizen, 'Unsteady natural convection in a partially heated rectangular cavity', *J. Heat Transfer* (in press).